



1 A new method to identify flux ropes in space plasmas

2 Shiyong Huang¹, Pufan Zhao¹, Jiansen He², Zhigang Yuan¹, Meng Zhou³, Huishan
 3 Fu⁴, Xiaohua Deng³, Ye Pang³, Dedong Wang¹, Xiongdong Yu¹, Haimeng Li⁴, Roy
 4 Torbert⁵, and James Burch⁶

5

6 ¹ School of Electronic Information, Wuhan University, Wuhan, China

7 ² School of Earth and Space Sciences, Peking University, Beijing, China

8 ³ Institute of Space Science and Technology, Nanchang University, Nanchang, China

9 ⁴ School of Space and Environment, Beihang University, Beijing, China

10 ⁵ University of New Hampshire, Durham, New Hampshire, USA

11 ⁶ Southwest Research Institute, San Antonio TX, USA

12

13 Abstract

14 Flux ropes are frequently observed in the space plasmas, such as magnetosphere,
 15 magnetosheath, and solar wind etc., and play an important role in the reconnection
 16 process and mass and flux transportation. One usually used bipolar signature and
 17 strong core field to identify the flux ropes. We propose here one new method to
 18 identify flux ropes based on the correlations between the variables of the data from
 19 in-situ spacecraft observations and the target-function-to-be-correlated (TFC) from
 20 the ideal flux rope model. Through comparing the correlation coefficients of different
 21 variables at different time and scales, and performing weighted average technique,
 22 this method can derive the scales and locations of the flux ropes. We discuss the
 23 limitation of our method and also compare it with other methods.

24

25 1. Introduction

26 Flux ropes, as one universal structure in the space plasma, are formed as a helical
 27 magnetic structure with magnetic field lines wrapping and rotating around a central
 28 axis (e.g., *Hughes and Sibeck*, 1987; *Slavin et al.*, 2003; *Zong et al.*, 2004; *Zhang et*
 29 *al.*, 2010). It is generally believed that flux ropes can be generated by magnetic
 30 reconnection in the eruptive energy processes, such as rapid variations of the



31 reconnection rate at a single X-line (e.g. *Nakamura and Scholer*, 2000; *Fu et al.*,
32 2013), multiple X-line reconnection (e.g. *Lee et al.*, 1985; *Deng et al.*, 2004). Flux
33 ropes play important roles in dissipating magnetic energy and controlling the
34 microscale dynamics of magnetic reconnection (e.g., *Drake et al.*, 2006; *Daughton et*
35 *al.*, 2007; *Fu et al.*, 2017). These structures are frequently observed and widely
36 studied recently in the magnetosphere, magnetosheath and solar wind (e.g. *Hu and*
37 *Sonnerup*, 2001; *Slavin et al.*, 2003; *Zong et al.*, 2004; *Zhang et al.*, 2010; *Huang et*
38 *al.*, 2012, 2014a, 2014b, 2015, 2016a, 2016b; *Rong et al.*, 2013). Many works have
39 tried to model flux rope from *in-situ* measurements based on the force-free
40 constant-alpha flux rope (e.g., *Lepping et al.*, 1990), non-force-free model (e.g.,
41 *Hidalgo et al.*, 2002), or the Grad-Shafranov equilibrium (e.g., *Hu and Sonnerup*,
42 2002).

43
44 Flux ropes embedded in current sheet are characterized by the bipolar signature of the
45 normal component of magnetic field, strong core field in the axis direction, and
46 enhancement in magnetic field strength. Therefore, one used negative-positive
47 (positive-negative) bipolar signature of the south-north magnetic field component in
48 the earthward (tailward) flow with an enhancement in the cross-tail component and
49 strength of magnetic field to identify flux rope in the magnetotail (e.g., *Slavin et al.*,
50 2003; *Huang et al.*, 2012). At the magnetopause, the bipolar variation is usually along
51 the sun-earth direction, and the core field is typically along the dawn-dusk direction
52 (e.g., *Zhang et al.*, 2010). However, flux ropes in the magnetosheath, which has been
53 reported recently by MMS (*Huang et al.*, 2016b), can move in any directions due to
54 the large fluctuations of the shocked solar wind. This leads to difficulty in identifying
55 the flux ropes there.

56
57 Several attempts are tried to survey flux ropes in the Earth's magnetotail by eyes
58 based on their signatures, such as bipolar variation of north-south magnetic field (e.g.,
59 *Richardson et al.*, 1987; *Slavin et al.*, 2003). Also, some methods are proposed to
60 automatically in some degrees survey the flux rope or flux transfer events (FTEs) via



bipolar field deflections (e.g., *Kawano and Russell*, 1996; *Vogt et al.*, 2010; *Jackman et al.*, 2014; *Smith et al.*, 2016). *Karimabadi et al.* (2009) have applied data mining technique (MineTool) to search FTEs using magnetic field and plasma data. Recently, *Smith et al.* (2017) developed a method to automatically detect cylindrically symmetric force-free flux ropes in the magnetotail only using magnetic field data. That method first locates the significant deflections in the north-south magnetic field component with peaks in the dawn-dusk component or total field. Then, the candidates are using Minimum Variance Analysis (MVA) to determine a local coordinate system. Finally, the candidates are fitted by a force-free model to determine whether they belong to flux ropes or not.

For some flux ropes with short duration, the plasma data have not enough high time resolution or even worse are not available. Thus the identification of flux ropes relies heavily on the magnetic field data. All aforementioned automatical methods are a bit complex, or require plasma data. Therefore, to identify flux rope only using the magnetic field data from single spacecraft, we propose a new and simple method based on the correlation coefficients between the signal and the ideal model of flux rope to identify flux ropes in space plasmas. The paper will be presented as follows: an introduction of the method in section 2; the test of the method on artificial data from the model in section 3; the applications of the method on the Cluster and MMS data in section 4; summary is given in section 5.

2. Approach

In this section, we simply introduce our method. Firstly, we derive target-function-to-be-correlated (TFC) from the ideal model of flux rope. Considering the variable and complicated observed flux ropes, we use the ideal non-force-free model of flux rope proposed by *Elphic and Russell* (1983), named as Elphic and Russell (E-R) Model because most of flux ropes with nonnegligible perpendicular current are not consistent with force-free model (e.g., *Hidalgo et al.*, 2002; *Zong et al.*, 2004; *Zhang et al.*, 2010; *Borg et al.*, 2012; *Huang et al.*, 2012,



2016b). This model is constructed with an intense core field inside of flux rope, which is shown in Figure 1. The equation of this model in the cylindrical coordinate (Y is defined as the axis orientation of flux rope) can be modified as below:

$$\begin{cases} B_y = B(r) \cos(\alpha(r)) \\ B_\phi = B(r) \sin(\alpha(r)) \\ B(r) = B_0 \exp(-r^2/b^2) \end{cases} \quad (1)$$

Where $\alpha(r) = \pi/2(1 - \exp(-r^2/a^2))$, B_y is the core field component, B_0 , a , and b are the constant, r is the radial distance to the flux rope center.

Figure 1 shows sketched diagram of the cylindrical flux rope from E-R model. For convenience, the rectangular coordinate is used in our analyses (shown in Figure 1). Y is the axis orientation of the flux rope, and the X - Z plane is the cross-section perpendicular to the axis orientation. X can be treated as sun-earth orientation, Y is the dawn-dusk orientation, and Z is similar to the south-north orientation in the magnetotail. If the one spacecraft cross the flux rope following the red path in Figure 1, B_z component will be characterized as bipolar signature, and B_y component has strong peak.

Figure 2 shows the observations when one virtual spacecraft cross the ideal flux rope (see spacecraft path in Figure 1). Here we assume the scale of flux rope as one unit, and 1 unite/s of moving speed of the spacecraft, thus set $a = 0.735$ s and $b = 0.735$ s, $B_0 = 10$ nT, and use the B_z as the bipolar variation component, B_y as the core field component, B_t as the total magnetic field. The center of the flux rope is located at 2.5 s. One can see the B_z bipolar signature, and the peak of core field and total magnetic field inside the flux rope.

Considering the previous observations, in which the B_z component during the crossing of the flux rope usually does not reach zero like that shown in Figure 2a, we cut out one part of the ideal flux rope as the TFC which is shown in Figure 3. The TFC is similar to the sinusoidal function when one performs Fast Fourier Transform (FFT)



analysis. We only used two components (B_y and B_z) and magnetic strength (B_t) as the TFC since only B_z and B_y components and B_t have very obvious typical feature usually from in-situ measurements (i.e., B_z has bipolar signature, B_y is strong core field, and B_t has peak inside flux rope), and B_x component has not common feature from observation viewpoint (e.g., *Slavin et al.*, 2003; *Huang et al.*, 2014a).

Secondly, we calculate the correlation coefficients between the signal and the TFC at different time and different scales. Before calculating the correlation coefficients, the amplitude of the TFC will be estimated from the signal. For example, the maximum value of B_t during the time interval is used as the amplitude of B_t in the TFC. The sliding time window is used in the calculation of the correlation coefficients. The calculated results of correlation coefficients are similar to the power spectral densities by FFT that displays the power spectral density at different time and different frequency. The higher values of the correlation coefficients, the more suitable for the description of the model on the signal.

Thirdly, we compare the correlation coefficients of the bipolar variation component B_z , core field component B_y , and total magnetic field B_t , and find out the high correlations (larger than the given threshold) at the same time and the same scale. This is due to that the bipolar signature in B_z , the enhancements of core field B_y and magnetic strength B_t should appear simultaneously with the same duration when one spacecraft cross the flux ropes.

Fourthly, we infer the location and the scale of the flux ropes based on the weighed average (it will be shown later), and the amplitude from minimum to maximum values of the bipolar variation.

3. Model test

One test is performed on the artificial data from E-R model plus the random noise. Figure 4 presents the test results. The test artificial data is shown in Figure 4a where



the noise is 10% of the amplitude of the flux rope. A series of the calculations are carried on B_z , B_y and B_t to obtain the correlation coefficients. One should point out that the absolute values of the correlation coefficients of B_z and B_y are given in Figure 4b and 4c respectively, because the bipolar structure can be positive-negative or negative-positive variation and the core field can be positive or negative. It can be seen that the correlation coefficients are largest at the scale of 0.6 ~ 1.5 s during the crossing of the flux rope (around *time* ~ 3.5 s).

We set the threshold as 0.9 to represent the results in Figure 5 where only the correlation coefficients with > 0.9 are displayed with black shadows. All correlation coefficients of the three variables have peaks at the *time* ~ 3.5 s with the time scale ~ 1 s. We use the weighted average technique (shown below) to identify the flux rope and estimate its time scale.

$$\tau = \sum coef_i \times \tau_i / \sum coef_i \quad (2)$$

where $coef_i$ is the correlation coefficient at time scale τ_i .

Figure 5e shows the estimated results. The crossing of the flux rope is marked with “1” and the duration is its scale, the center of the flux rope is at the center of the line. In this test, the scale is estimated as 1.039 s, the location is 3.496 s. The amplitude is estimate as 4.43 nT from minimum to maximum values of the bipolar variation. Aforementioned sets, one can estimate the error of the scale as 3.9%, i.e., $(1.039-1.0)/1.0 = 3.9\%$. Therefore, our method can successfully identify the flux rope, and estimate its scale, location and amplitude.

4. Application

In this section, we apply our new method to the spacecraft measurements in the magnetosheath and the magnetotail.

4.1 Flux rope in the magnetosheath

Flux ropes are successfully identified in the magnetosheath using the unprecedented



179 high resolution data from Magnetospheric Multiscale (MMS) (*Burch et al.*, 2016)
 180 mission (*Huang et al.*, 2016b). Their observations demonstrate that highly dynamical,
 181 strong wave activities and electron-scale physics occur in the magnetosheath ion-scale
 182 flux ropes. Figure 6 gives the observations of ~ 14 s from MMS2 on 25 Oct 2015 and
 183 the test results of our method. Similar to the model test, we use the same variables to
 184 present the components of the bipolar variation, core field and total magnetic field
 185 after transformed to minimum variable analysis (MVA) analysis (*Huang et al.*,
 186 2016b). The threshold of the correlation coefficients is also set as 0.9 in Figure 6. We
 187 can see that the correlation coefficients of the three variables (Figure 6b-6d) only have
 188 high values at the same time around $time = 5.5$ s, implying that one flux rope is
 189 identified by this method. Based on the weighted average method in equation (2), the
 190 time scale of the flux rope is 1.11 s, and its central location is at 5.38 s. The amplitude
 191 is estimate as 115 nT. All these results are consistent with previous findings from
 192 multi-spacecraft data in *Huang et al.* (2016b).

193

194 4.2 Flux rope in the magnetotail

195 Flux ropes are frequently observed in the magnetotail, and play an important role
 196 during magnetic reconnection and magnetotail dynamic (e.g., *Slavin et al.*, 2003;
 197 *Zong et al.*, 2004; *Chen et al.*, 2008; *Huang et al.*, 2012, 2016a; *Fu et al.*, 2015, 2016).
 198 *Chen et al.* (2008) have identified several flux ropes filled with energetic electrons
 199 during magnetic reconnection on 10 Jan 2001 by using the Cluster data. Figure 7
 200 shows the magnetic field in GSM coordinates from the Cluster mission (*Escoubet et*
 201 *al.*, 1997) in the magnetotail and the application results of our method. There are
 202 several bipolar variations in B_z during this time interval (Figure 7a). Figures 7b-7d
 203 present the correlation coefficients (larger than 0.9 of the threshold) of the three
 204 variables. Here we try to identify small-scale flux ropes, so that we perform the
 205 method only at short time scale. There are full of high correlation coefficients (grey
 206 shadows) in Figures 6b-6d. After compare with the correlation coefficients at the
 207 same time and same scale, our method resolves three possible flux ropes in Figure 7e.
 208 The results are summarized in Table 1. The three structures are close to ideal flux



209 rope with bipolar signature in B_z , and peaks in core field B_y and total magnetic field B_t .
 210 All three flux ropes identified by our method have been reported in *Chen et al.*
 211 (2007).

212

213 We should point out that our method only can identifies the flux rope and derives its
 214 duration. If the plasma velocity data is available, then we can estimate the actual
 215 spatial scale of the flux rope. If multi-spacecraft data are available for the time
 216 interval of interest, one can derive the size, the orientation, and the motion of the flux
 217 rope using by the multi-spacecraft method such as *Sonnerup et al.* (2004), *Shi et al.*
 218 (2005, 2006) and *Zhou et al.* (2006a, 2006b). However, the separation of the Cluster
 219 was much larger than the size of the flux ropes on 01 October 2001, implying that one
 220 cannot use multi-spacecraft method here.

221

222 **5. Summary and Discussion**

223 In summary, we developed a new method to identify flux ropes in the space plasmas.
 224 This method is based on the correlation coefficients between the signal and the TFC
 225 from E-R model. If the correlation coefficients of three variables (B_z , B_y and B_t) of the
 226 signal have high values of correlation coefficients at the same time and same scale,
 227 one can deduce the existence of one flux rope and estimate its location and its time
 228 scale (i.e., the duration). The tests on the artificial data and the in-situ realistic
 229 spacecraft data show that our method can successfully search out the flux ropes and
 230 obtain their locations and time scales.

231

232 Bipolar variation in B_z component and the enhancement in core field and magnetic
 233 field strength are the typical signatures for most of flux rope. But it doesn't mean that
 234 all observations from any crossing of the spacecraft would have those signatures,
 235 which depends on the spacecraft trajectory. However, one only can select or identify
 236 the flux rope showing the typical signatures, and miss other flux rope not having the
 237 typical signatures. Some special field structures may induce the similar signatures
 238 along some special trajectories. But we thought this opportunity is too few in the



239 magnetotail. However, one can use the plasma measurements to rule out this
 240 possibility.

241

242 Aforementioned attempts are used to identify flux ropes in the Earth's magnetotail by
 243 eyes or half-automatically based on the bipolar variation of (e.g., *Richardson et al.*,
 244 1987; *Slavin et al.*, 2003; *Kawano and Russell*, 1996; *Vogt et al.*, 2010; *Jackman et al.*,
 245 2014; *Smith et al.*, 2016). *Karimabadi et al.* (2009) used data mining technique
 246 (MineTool) to search flux ropes using both magnetic field and plasma data. That
 247 method is too complex to apply in the data analysis. *Smith et al.* (2017) proposed one
 248 method to automatically detect force-free flux ropes based on magnetic field data
 249 from single spacecraft. In present study, we used the TFC derived from non-force-free
 250 flux rope model to calculate the correlation coefficients with the signal, and then
 251 compare the large correlation coefficients of different variables to identify the flux
 252 rope. Our method is flexible and easy to apply in the in-situ spacecraft data compared
 253 with other methods. We will quantitatively model the flux ropes identified by our
 254 method and derive more information of the flux ropes.

255

256 We should point out that there are several limitations in our method.

257 1. Our method can only detect the nearly ideal cylindrical flux rope since we used
 258 non-force-free E-R model to describe the TFC, which limits the application of this
 259 method. The non-force-free model proposed by E-R is just one possible solution of all
 260 the flux rope that satisfies $\mathbf{J} \times \mathbf{B} \neq 0$. Actually one can use the other flux rope models to
 261 replace E-R model, and extend our method to identify the flux ropes.

262

263 2. If the flux ropes are not well regular, there are large time deviations between B_z , B_y
 264 and B_t which will lead to miss of some flux ropes when we apply the method.

265

266 3. The threshold value of correlation coefficients can affect the results. When the
 267 threshold value is too small that the method finds out some possible structures which
 268 do not belong to flux ropes, or too large that the method will miss some flux ropes.



269

270 4. The correlation coefficients at small scale (especially in B_y and B_t) could be very
 271 large, which may affect our results. The method may find some possible structures
 272 related to such fluctuations. We will improve this method and apply it to detect the
 273 flux ropes in the turbulent magnetosheath in the future.

274

275

276 Acknowledgement

277 We thank the entire Cluster and MMS team and instrument leads for data access and
 278 support. This work was supported by the National Natural Science Foundation of
 279 China (41374168, 41404132, 41574168, 41674161), Program for New Century
 280 Excellent Talents in University (NCET-13-0446), and China Postdoctoral Science
 281 Foundation Funded Project (2015T80830). MMS Data is publicly available from the
 282 MMS Science Data Center at <http://lasp.colorado.edu/mms/sdc/>. Cluster Data is
 283 publicly available from the Cluster Science Archive at
 284 <http://www.cosmos.esa.int/web/csa>.

285

286 Reference

- 287 Borg, A.L., Taylor, M.G.G.T., and Eastwood, J.P. (2012), Observations of magnetic
 288 flux ropes during magnetic reconnection in the Earth's magnetotail, Ann. Geophys.,
 289 30, 761-773, doi:10.5194/angeo-30-761-2012
- 290 Burch, J. L., T. E. Moore, R. B. Torbert, and B. L. Giles (2015), Magnetospheric
 291 Multiscale overview and science objectives, Space Sci. Rev., 199, 5,
 292 doi:10.1007/s11214-015-0164-9
- 293 Chen, L.-J., et al. (2007), Observation of energetic electrons within magnetic islands,
 294 Nature Phys., 4, 19 – 23, doi:10.1038/nphys777.
- 295 Deng, X. H., H. Matsumoto, H. Kojima, T. Mukai, R. R. Anderson, W. Baumjohann,
 296 and R. Nakamura (2004), Geotail encounter with reconnection diffusion region in the
 297 Earth's magnetotail: Evidence of multiple X lines collisionless reconnection?, J.
 298 Geophys. Res., 109, A05206, doi:10.1029/2003JA010031.



- 299 Elphic, R. C., and C. T. Russell (1983), Magnetic Flux Ropes in the Venus
 300 Ionosphere: Observations and Models, *J. Geophys. Res.*, 88(A1), 58–72,
 301 doi:10.1029/JA088iA01p00058.
- 302 Escoubet, C. P., R. Schmidt, and M. L. Goldstein (1997), Cluster—Science and
 303 mission overview, *Space Sci. Rev.*, 79, 11–32.
- 304 Fu, H. S., et al. (2013), Dipolarization fronts as a consequence of transient
 305 reconnection: In situ evidence, *Geophys. Res. Lett.*, 40, 6023–6027,
 306 doi:10.1002/2013GL058620.
- 307 Fu, H. S., A. Vaivads, Y. V. Khotyaintsev, V. Olshevsky, M. André, J. B. Cao, S. Y.
 308 Huang, A. Retinò, and G. Lapenta (2015), How to find magnetic nulls and reconstruct
 309 field topology with MMS data?, *J. Geophys. Res. Space Physics*, 120, 3758–3782. doi:
 310 10.1002/2015JA021082.
- 311 Fu, H. S., et al. (2016), Identifying magnetic reconnection events using the FOTE
 312 method, *J. Geophys. Res. Space Physics*, 121, 1263–1272,
 313 doi:10.1002/2015JA021701.
- 314 Fu, H. S., A. Vaivads, Y. V. Khotyaintsev, M. André, J. B. Cao, V. Olshevsky, J. P.
 315 Eastwood, and A. Retinò (2017), Intermittent energy dissipation by turbulent
 316 reconnection, *Geophys. Res. Lett.*, 44, 37–43, doi:10.1002/2016GL071787.
- 317 Hidalgo, M. A., C. Cid, A. F. Vinas, and J. Sequeiros, A non-force-free approach to
 318 the topology of magnetic clouds in the solar wind, *J. Geophys. Res.*, 106(A1),
 319 10.1029/2001JA900100, 2002.
- 320 Hu, Q., and B. U. O. Sonnerup, Reconstruction of magnetic flux ropes in the solar
 321 wind, *Geophys. Res. Lett.*, 28, 467 – 470, 2001
- 322 Hu, Q., and B. U. O. Sonnerup, Reconstruction of magnetic clouds in the solar wind:
 323 Orientations and configurations, *J. Geophys. Res.*, 107(A7),
 324 doi:10.1029/2001JA000293, 2002.
- 325 Huang, S. Y., et al. (2012), Electron acceleration in the reconnection diffusion region:
 326 Cluster observations, *Geophys. Res. Lett.*, 39, L11103, doi:10.1029/2012GL051946.
- 327 Huang, S. Y., et al. (2014a) Observation of directional change of core field inside flux
 328 ropes within one reconnection diffusion region in the Earth’s magnetotail, *Chin. Sci.*



- 329 Bull. DOI 10.1007/s11434-014-0583-0
- 330 Huang, S. Y., M. Zhou, Z. G. Yuan, X. H. Deng, F. Sahraoui, Y. Pang, and S. Fu
 331 (2014b), Kinetic simulations of electric field structure within magnetic island during
 332 magnetic reconnection and their applications to the satellite observations, J. Geophys.
 333 Res. Space Physics, 119, 7402–7412, doi:10.1002/2014JA020054
- 334 Huang, S. Y., et al. (2015), Kinetic simulations of secondary reconnection in the
 335 reconnection jet, J. Geophys. Res. Space Physics, 120, doi:10.1002/2014JA020969
- 336 Huang, S. Y., et al. (2016a), In situ observations of flux rope at the separatrix region
 337 of magnetic reconnection, J. Geophys. Res. Space Physics, 121, 205–213,
 338 doi:10.1002/2015JA021468.
- 339 Huang, S. Y., et al. (2016b), MMS observations of ion-scale magnetic island in the
 340 magnetosheath turbulent plasma, Geophys. Res. Lett., 43, 7850–7858,
 341 doi:10.1002/2016GL070033.
- 342 Karimabadi, H., T. B. Sipes, Y. Wang, B. Lavraud, and A. Roberts (2009), A new
 343 multivariate time series data analysis technique: Automated detection of flux transfer
 344 events using Cluster data, J. Geophys. Res., 114, A06216,
 345 doi:10.1029/2009JA014202.
- 346 Khrabrov, A. V., and B. U. O. Sonnerup, DeHoffmann-Teller Analysis, in Analysis
 347 Methods for Multi-Spacecraft Data, edited by G. Paschmann and P. W. Daly, chap. 9,
 348 pp.221-248, Int. Space Sci. Inst., Bern, Switzerland, and Eur. Space Agency, Paris,
 349 France, 1998.
- 350 Lee, L. C., Z. F. Fu, and S.-I. Akasofu (1985), A simulation study of forced
 351 reconnection processes and magnetospheric storms and substorms, J. Geophys. Res.,
 352 90(A11), 10,896–10,910.
- 353 Lepping, R. P., J. A. Jones, and L. F. Burlaga, Magnetic field structure of
 354 interplanetary magnetic clouds at 1 AU, J. Geophys. Res., 95, 11,957-11,965, 1990.
- 355 Nakamura, M. and M. Scholer (2000), Structure of the magnetopause reconnection
 356 layer and of flux transfer events: Ion kinetic effects, J. Geophys. Res., 105(A10),
 357 23,179–23,191, doi:10.1029/2000JA900101.
- 358 Rong, Z. J., W. X. Wan, C. Shen, T. L. Zhang, A. T. Y. Lui, Y. Wang, M. W. Dunlop,



- 359 Y. C. Zhang, and Q.-G. Zong (2013), Method for inferring the axis orientation of
360 cylindrical magnetic flux rope based on single-point measurement, *J. Geophys. Res.*
361 *Space Physics*, 118, 271–283, doi:10.1029/2012JA018079.
- 362 Slavin, J. A., Lepping, R. P., Gjerloev, J., Fairfield, D. H., Hesse, M., Owen, C. J.,
363 Moldwin, M. B., Nagai, T., Ieda, A., and Mukai, T. (2003), Geotail observations of
364 magnetic flux ropes in the plasma sheet, *J. Geophys. Res.*, 108, 1015–1032.
- 365 Shi, Q. Q., C. Shen, Z. Y. Pu, M. W. Dunlop, Q.-G. Zong, H. Zhang, C. J. Xiao, Z. X.
366 Liu, and A. Balogh, Dimensional analysis of observed structures using multipoint
367 magnetic field measurements: Application to Cluster, *Geophys. Res. Lett.*, 32,
368 L12105, doi:10.1029/2005GL022454, 2005.
- 369 Shi, Q. Q., C. Shen, M. W. Dunlop, Z. Y. Pu, Q.-G. Zong, Z.-X. Liu, E. A. Lucek,
370 and A. Balogh, Motion of observed structures calculated from multi-point magnetic
371 field measurements: Application to Cluster, *Geophys. Res. Lett.*, 33, L08109,
372 doi:10.1029/2005GL025073, 2006.
- 373 Smith, A. W., C. M. Jackman, and M. F. Thomsen (2016), Magnetic reconnection in
374 Saturn’s magnetotail: A comprehensive magnetic field survey, *J. Geophys. Res. Space*
375 *Physics*, 121, 2984–3005, doi:10.1002/2015JA022005.
- 376 Smith, A. W., J. A. Slavin, C. M. Jackman, R. C. Fear, G.-K. Poh, G. A. DiBraccio, J.
377 M. Jasinski, and L. Trenchi (2017), Automated force free flux rope identification, *J.*
378 *Geophys. Res. Space Physics*, 122, 780–791, doi:10.1002/2016JA022994.
- 379 Sonnerup, B. U. O., H. Hasegawa, and G. Paschmann, Anatomy of a flux transfer
380 event seen by Cluster, *Geophys. Res. Lett.*, 31, L11803, doi:10.1029/2004GL020134,
381 2004.
- 382 Zhou, X.-Z., Q.-G. Zong, Z. Y. Pu, T. A. Fritz, M. W. Dunlop, Q. Q. Shi, J. Wang,
383 and Y. Wei, Multiple triangulation analysis: another approach to determine the
384 orientation of magnetic flux ropes, *Ann. Geophys.*, 24, 1759–1765, 2006a.
- 385 Zhou, X.-Z., Q.-G. Zong, J. Wang, Z. Y. Pu, X. G. Zhang, Q. Q. Shi, and J. B. Cao,
386 Multiple triangulation analysis: application to determine the velocity of 2-D structures,
387 *Ann. Geophys.*, 24, 3173–3177, 2006b.
- 388 Zong, Q.-G., et al. (2004), Cluster observations of earthward flowing magnetic island



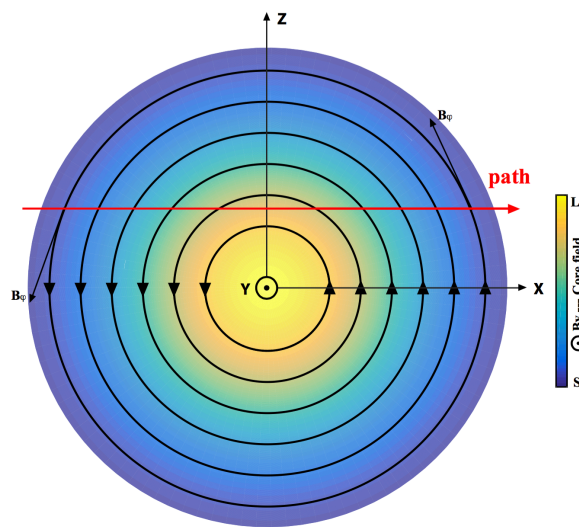
389 in the tail, Geophys. Res. Lett., 31, L18803, doi:10.1029/2004GL020692.
 390 Zhang, H., et al. (2010), Evidence that crater flux transfer events are initial stages of
 391 typical flux transfer events, J. Geophys. Res., 115, A08229, doi:10.1029/2009JA01
 392 5013.
 393
 394
 395
 396
 397
 398
 399 Table 1. The location, sale and amplitude of the flux ropes identified by the method.
 400 The amplitude is defined as the values of the bipolar variation from minimum to
 401 maximum.

# of flux rope	1	2	3
Location [s]	37.91	113.79	127.93
Scale [s]	1.99	2.84	2.05
Amplitude [nT]	9.96	20.49	12.59

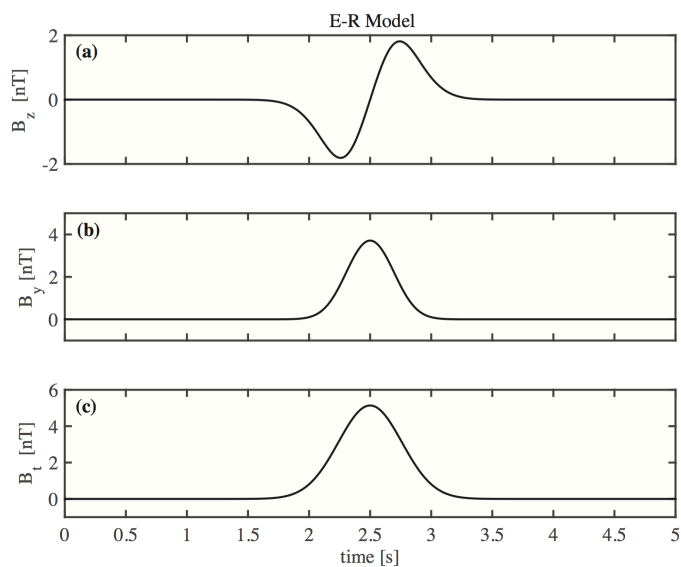
402
 403
 404
 405
 406
 407
 408
 409
 410
 411
 412
 413



414
415
416
417 **Figure captions**
418

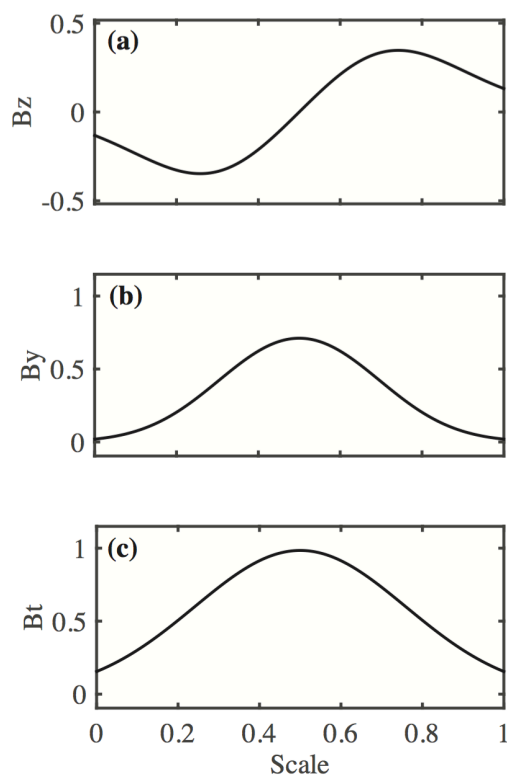


419
420 Figure 1. Sketched diagram of the cylindrical flux rope. The flux rope is right-hand
421 handedness structure. The black circled lines are the magnetic field lines. The red
422 arrow is the projection of spacecraft path. The rectangular coordinate is used in our
423 analyses. Y is the axis orientation of the flux rope, and the X-Z plane is the
424 cross-section perpendicular to the axis orientation. The core field is out-of-plane, and
425 the color represents the relative strength of core field (yellow: large, blue: small).
426



427
 428 Figure 2. The three variables B_z (a), B_y (b), and B_t (c) of the ideal cylindrical flux rope
 429 described by E-R model.

430

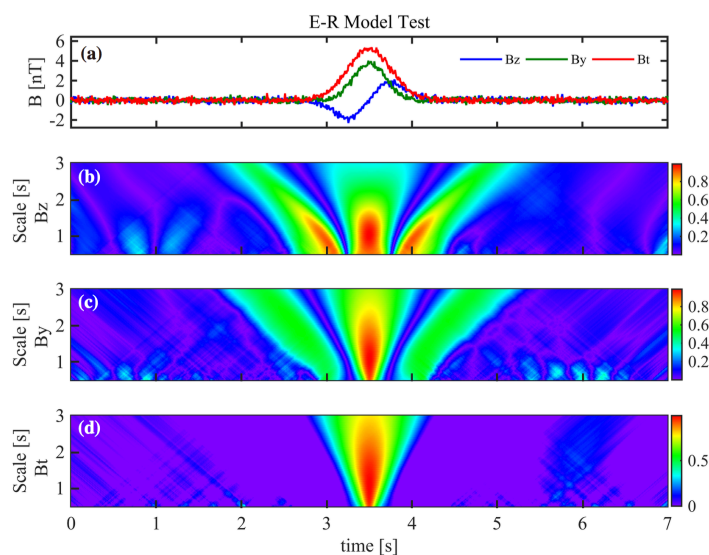


431
 432 Figure 3. The target-function-to-be-correlated (TFC) derived from E-R model. The
 433 amplitudes and scale are dimensionless.

434

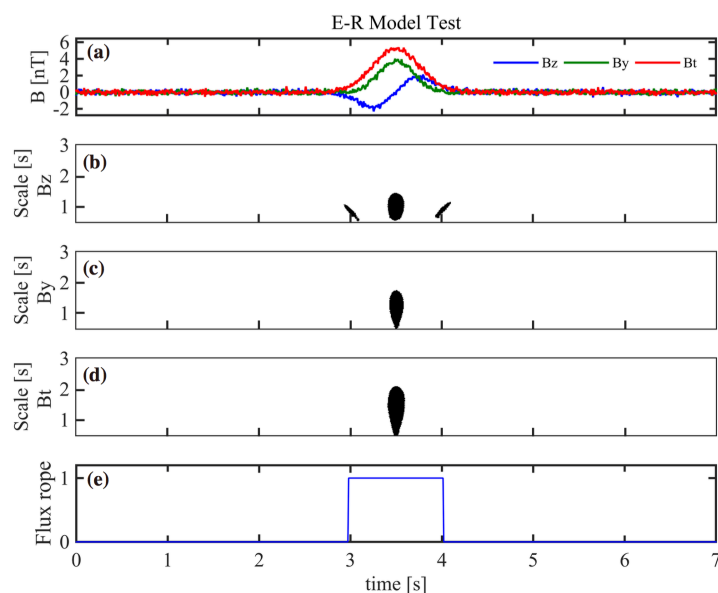
435

436



437
 438 Figure 4. The test results on E-R model. (a) three variables B_z , B_y , and B_t from E-R
 439 model with 10% random noise; (b-d) the correlation coefficients between the
 440 variables of B_z , B_y , and B_t and the TFC shown in Figure 3, respectively.

441
 442
 443
 444



445
 446 Figure 5. The test results on E-R model with a threshold 0.9. (a) three variables B_z , B_y ,
 447 and B_t from E-R model with 10% random noise; (b-d) the correlation coefficients
 448 (≥ 0.9) between the variables of B_z , B_y , and B_t and the TFC, respectively; (e) the index
 449 when the virtual spacecraft cross the flux rope (if the spacecraft cross the flux rope,
 450 the index is 1; if not, the index is 0). The duration of the index presents the time scale
 451 of the flux rope.

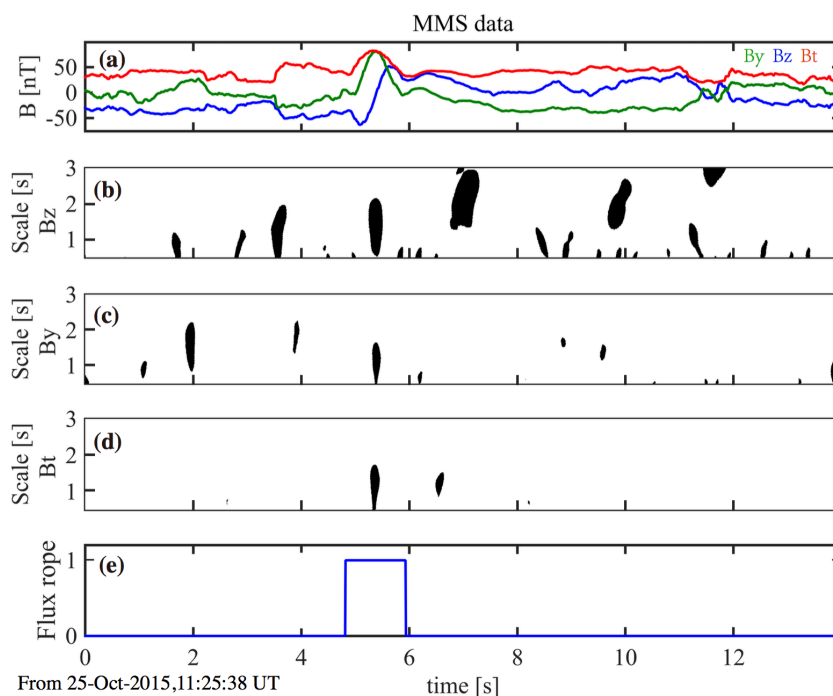
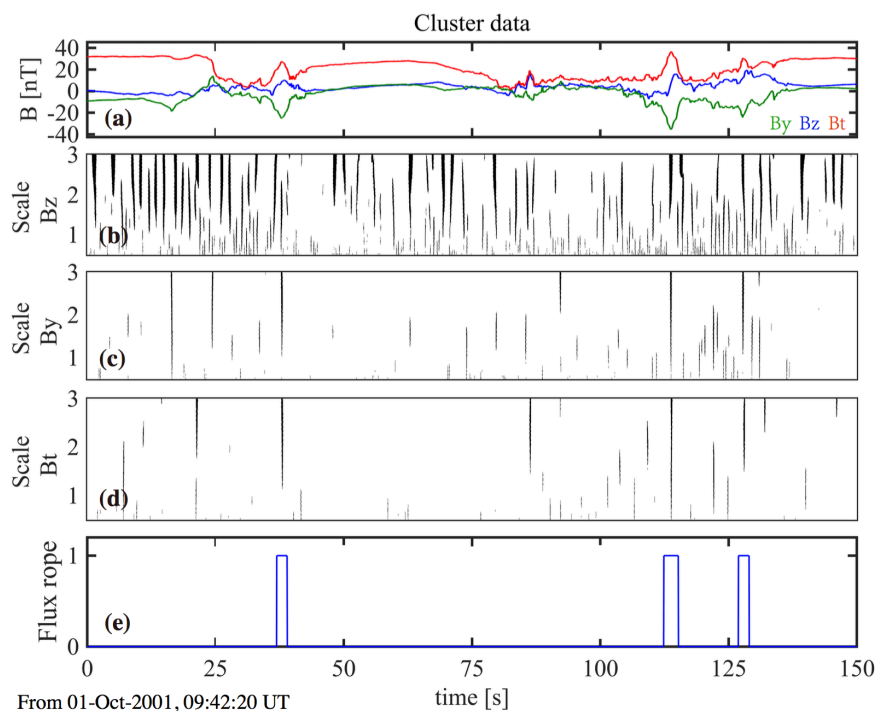


Figure 6. Testing the method on MMS data in the magnetosheath. The same format as in Figure 5.



458 From 01-Oct-2001, 09:42:20 UT
 459 Figure 7. Testing the method on Cluster data in the magnetotail. The same format as
 460 in Figure 5.